Solidification of Trapped Liquid in Rocks and Crystals

Revision 2 December 15, 2012

S. A. MORSE*

Department of Geosciences, University of Massachusetts, 611 North Peasant St., Amherst, Massachusetts 01003-9297, U. S. A.

*E-mail: tm@geo.umass.edu

ABSTRACT

Trapped liquid in an igneous cumulate solidifies over a range of time and temperature that can be retrieved by use of the lever rule in binary solutions applied to plagioclase using the range in the An content found for the individual rock studied. The An range, so called, when measured in sufficient detail, defines the solidification history. The instantaneous solid composition along the solidus defines the zoning of the plagioclase as it follows the trapped liquid on the liquidus. The reference bulk composition of the trapped liquid is given by an intercept on the initial solid-liquid lever, defined by the fraction of plagioclase in the trapped parent magma times the residual porosity. The mafic fraction is assumed to solidify by reaction independently of the plagioclase zoning. The residual porosity is estimated from the content of evolved components in the trapped liquid and can also be calculated from the An range itself when that is calibrated to a value independently determined from the evolved components. Examples from a recent treatment of residual porosity are given for the solidification of selected rock compositions from the Kiglapait and Skaergaard intrusions. The same principles apply to the solidification of melt inclusions, with the difference that the latter tends to sample an evolved sheath by capture, rather than a parent magma trapped by closure of a cumulate, because only the cumulate has had time to exchange the evolved rejected solute owing to its slow solidification. Experimental examples of melt inclusions trapped at liquidus conditions demonstrate the highly evolved composition of the sheath compared to the bulk glass composition. The application of the solidification principle to presumed liquid immiscibility in the Skaergaard intrusion suggests that the melt inclusions are evolved during the capture process and then solidified as given by the An range in the plagioclase. The hypothesis of liquid immiscibility is not needed in this analysis. The very different end-stage feldspar histories of the two intrusions is attributed to the sequestering of low-melting feldspar components in the trapped liquids of the Skaergaard cumulates, compared to the lesser amounts trapped in the Kiglapait cumulates.

Keywords: Solidification, cumulates, trapped liquid, residual porosity, melt inclusions, An range, Kiglapait, Skaergaard, end-stage histories.

INTRODUCTION

In response to a recent contribution about the An range of plagioclase and residual porosity in the Kiglapait and Skaergaard intrusions (Morse, 2012), an interested reader asked to know the assumed physics of how trapped liquid solidifies in the context of the An range. This is a reasonable question, given the range of alternatives. The hoped-for alternative, it developed, was that the trapped liquid would fractionate to the limit of a binary loop, so the true An range would always approximate to the initial plagioclase composition An(I) minus (~An_0), and hence only be a function of nominal stratigraphic height. In such a case, there would presumably be no correlation between An range and the residual porosity of a given individual rock sample, which was the goal of the cited study.

Clearly, the substance of the reader's argument was that the measured values of An range were all defective by failing to discover the most evolved plagioclase composition in the rock. This supposition was supported by the finding that very evolved rims could be found in rocks of the Skaergaard intrusion (Humphreys, 2009) in which the most evolved rim was An_{31}, not by any means the limit of An_0 but perhaps close to the end-stage of Skaergaard fractionation.

The alternative proposition is that the observed An range and its correlation with independently determined residual porosity *defines* the physics of solidification of trapped liquid. If the An range truly misses some lower values because of the size-range truncation, the correlation would still be present, but with a different equation. In this paper we explore the history of how a cumulate becomes finally solidified.

CONSIDERATIONS

There are at least three stages in the formation of an igneous cumulate. **First** is the assembly of crystals at the floor of the contemporaneous magma body to make a packing fraction of at least 50%, which is close to the mechanical criterion for a solid. In practice for troctolitic liquids we find evidence for values at least as high as 74% and possibly as high as 85% (Morse, 2012 Fig, 14). This paper is not about that stage.

The **second stage** involves some maturation of the cumulate by continued crystal growth at

constant plagioclase composition. Because plagioclase is a refractory mineral that cannot equilibrate in a dry magma (Morse, 1984; Grove et al. 1984), its composition history is taken as reflecting the thermal history of the intercumulus liquid. If there is continued growth at constant composition the history is taken to be isothermal during that time. If isothermal growth occurs, it requires the coupled exchange reaction: $CaAl(NaSi)_{-1}$, where the first couple is inbound and the second couple outbound with reference to the cumulate versus the external magma. Alternatively if the crystal mush is tens to hundreds of meters deep (M^{c}Kenzie, 2011) the cumulate may be compressed and compacted with physical expulsion of the melt. This paper does not concern this stage in either of the scenarios depicted.

The **third stage** in the life of an igneous cumulate is the **completion of solidification** indicated by zoning of plagioclase and caused by the absence of the exchange reaction. Taking such zoning as *prima facie* evidence of evolving and evolved resident liquid, the cumulate system is now declared CLOSED in the strict thermodynamic sense and that *and only that* is what this paper is about.

Following convention, we call the parent of all the zoned plagioclase **trapped liquid**, which is identical in mass and composition to what we call the **residual porosity**.

PREVIOUS WORK

Residual porosity

The residual porosity (p_r) in the Kiglapait Lower Zone (Morse, 1979) was determined by dividing the mode of an excluded component in the rock by the calculated mode of that component in the summation liquid. For the first 90 percent of the intrusion solidified (90 PCS) the result is given as $p_r = 0.139 \pm 0.007 \times F_L^{0.91}$, where F_L is the fraction of liquid remaining (Morse, 1979; 2012, where this matter is discussed at length).

Measurement of the An range

As described at length in Morse (2012) this quantity, the An range, was measured by electron probe analysis in grain mounts representing ~100 g of hand specimen or drill core. The sample volume investigated is approximately 10^4 times that of a standard thin section.

Conversion to residual porosity

The variation of the An range with PCS at the present exposure level is given by $Y = -0.062(PCS) + 9.91$ where Y is the An range in mol %, shown to be highly significant at the 95% confidence interval (Morse 2012 Fig. 9a). When the two stratigraphic variations for porosity and An range are combined, the % residual porosity = 2.19*An range -7.61 for An range > 3.5 %, else = 0 (see Fig. 8b of Morse 2012). This equation gives the results of the residual porosity *for individual samples* at all stratigraphic heights in the intrusion. For clarity in this discussion the stratigraphically - ordered results are shown here in Fig. 1, modified from Fig. 11 of that reference. The figure shows an abundance of porosities near zero and all of these are interpreted to define adcumulates that serve as impermeable barriers to any melt existing above or below. These impermeable barriers are calculated (Morse 2012 p. 913) to occur as frequently as every 1.3 to 15 m, hence an order of magnitude closer together than the thickness of crystal mush needed for compaction.

PETROGRAPHY

The ground truth of petrology is founded on the observation of thin sections of rock that reveals many features of texture and abundance of the constituent minerals. Of particular notice here is the fact that plagioclase zoning is highly visible under crossed polars and easily quantified by electron microprobe. The basis of this discussion is the An range of plagioclase as determined in grain mounts representing a hand specimen or drill core, as described in Morse (2012). That document also contained a description of 38 visual petrographic observations that correlated what was seen with what was measured. The results were summarized in Table 2 of that paper, in which the transition from pre-cumulus to endo-cumulus zoning was defined.

There are some 800 thin sections of the Kiglapait intrusion that have been and continue to be scrutinized for all aspects of the intrusion's petrography. Most of these from the Lower and Upper Zones are known to show, in small quantity, strong *reversed* rims on plagioclase. As originally described (Morse and Nolan, 1984) these can in some instances reach reversals as high as 32 mol % An. Reversed rims are also found in the Skaergaard intrusion (Humphreys, 2009). Comparison of optical observations and analytical dispersion suggests that the strong reversals are rarely captured in the grain mounts. It is also probable that some low values of An also escape the grain mount analyses. Does this mean that the grain mounts systematically under-represent evolved plagioclase compositions? The answer from petrography is a decided

NO, for the following reasons.

In the Kiglapait intrusion the feldspar stages run from plagioclase to antiperthite at An_{35} to mesoperthite at An_{20} to spectacularly resorbed and unmixed ternary feldspars at $An_{15\text{-}5}$ at the end of crystallization (see examples in Figs. 7-8 in Morse, 2012). Stage 2 (antiperthite) first appears at 97 PCS (volume percent solidified); stage 5 (all mesoperthite) appears at 99.9 PCS and the final stages near 99.97 PCS. Hence when we discuss all the grain-mount data on the An range below 97 PCS there is no possibility of finding a low An content < 35 mol % without also seeing it in thin section. ~~(The specific data cited here are unpublished but in preparation for publication. The overall feldspar trend is described by Speer and Ribbe, 1973.)~~ (See images in Morse, 1969 and Morse, 2012.) The late stages of solidification are therefore described adequately by the observed An range, which is not infected by invisible low-An grains.

SYSTEMATICS OF SOLIDIFICATION

Assumptions

The strict thermodynamic sense of a closed system mentioned above requires a constant bulk composition for the system, with no exchange to the surroundings, a condition that is, in this case, defined by the sum of the crystalline cumulate and the residual porosity. The plagioclase in the cumulate is assumed to be isocompositional and defined by the upper limit of the An range. The plagioclase composition of the trapped liquid is the integral of all crystal zoning down to the lower limit of the An range. This history is solved graphically on the binary loop.

The physical and chemical system defined here is the hand specimen or drill core actually sampled. Pressure is taken as constant and temperature is taken as variable. It turns out that the An range is capable of defining the temperature range over which a trapped liquid has solidified, given appropriate experimental results bearing on the range of bulk compositions encountered. This limited thermometry is an added bonus to this investigation.

Principle

If the An range scales with residual porosity, as shown in above, then it must *define* the

process of solidification in the trapped liquid. This simple conclusion follows from the fact that when the An range is zero (ignoring any pre-cumulus effect) the residual porosity is zero, and at the lower limiting value of the An range, the system is solid and the total solid composition has reached the bulk composition. If this were not so, the An range would have to be larger.

The principle is conveniently illustrated with a simple phase diagram of a binary loop, Fig. 2, chosen to be abnormally fat (K_D = 0.2; Morse, 2000) for clarity of illustration. The bulk composition of the trapped liquid is defined by the residual porosity, here set at 0.25. The lever shown has an "*l*" leg equal to 25 % of the whole length. The An range defines the history, from start to finish, of solidification, which occurs by cooling of trapped liquid and production of the instantaneous solid composition ISC ("xl zoning") along the solidus. The reaction progress is indicated by the diminishing length of the "*l*" leg, which runs from the total solid composition (TSC) to the bulk composition. Of this series, only the final lever to the BC is shown. In the figure the TSC path is arbitrarily drawn to approximate the paths calculated by Rayleigh fractionation (Morse, 1997), with the constraint that it must start at the initial solidus composition and follow towards (but always behind) the solidus until it arrives at the bulk composition.

It may be helpful to consider the history behind the snapshot situation of Fig. 2. If this were a normal textbook exercise it would begin at high temperature where the bulk composition BC intersects the liquidus. Then the liquid would have run down along the liquidus and the crystals down along the solidus until they arrived at the present configuration. At this point, assuming perfect equilibrium crystallization (which is impossible with plagioclase!), there would be 75 % crystals of composition given by end of the lever at the solidus, and 25 % liquid at the liquidus. In the present case, however, all the crystals have physically arrived into the cumulate having a constant composition and formed at a constant temperature from an effectively infinite reservoir. (There may have been an episode of adcumulus growth at constant *T, P, X* to bring the system from a larger initial porosity to the present 25%.)

So now the starting point of the exercise is one in which the crystals are delivered, without any memory of the prior history (if any existed). It is the exact same result as the conventional equilibrium crystallization history, but the crystals have grown elsewhere at constant composition instead of having to have been (impossibly) reacted to their present composition.

The mother liquid being trapped thinks all those crystals are hers, and she is morally justified in thinking so in that she is simply the last packet from the infinite reservoir. And she is

depleted compared to the original liquid at the higher liquidus, and therefore has only a limited amount of plagioclase left to crystallize.

The next crystallization step, however, will be one of fractionation in which the plagioclase crystals become zoned until their aggregate composition (the TSC) reaches the BC. That end point is defined by the lower limit of the An range.

Application

The analysis above is incomplete in that it ignores the role of the mafic components of the trapped liquid. These are assumed to crystallize by reactive batch crystallization, or in the case of augite, possibly by crystallization at constant composition. In any case, they have no effect on the evolution of the plagioclase composition, which is the indicator of when the process ends. Therefore, in the further diagrams, the residual porosity is partitioned according to the mass fraction of feldspar in the contemporary magma at the time the liquid was trapped, recalling that the adcumulus growth process has refreshed the intercumulus liquid from this source until the moment of trapping. The fraction of feldspar in the contemporary magma is estimated from the stratigraphic position of the rock and calculated from the CIPW norm. In the Skaergaard case it is estimated from the zone averages listed by McBirney (1996).

Kiglapait examples

Figure 3 shows two examples of the calculation for the maximum orthocumulates from the Kiglapait intrusion in which the An range is large, both in the basal Lower Zone at 13 PCS and in the uppermost Upper Zone (strictly, the UZ-UBZ sandwich horizon) at 99.99 PCS, for which a photomicrograph is shown in Fig. 8b of Morse (2012). The plagioclase loop is drawn in this figure for a linear partitioning value of $K_D = 0.416$ consistent with a mean pressure of 3 kbar using the relation $K_D = 0.516P + 0.262$ for P in kbar (Morse et al., 2004; McIntosh, 2009). ~~unpublished data)~~. Each example is identified by sample number and PCS value, the residual porosity calculated from the An range, the feldspar fraction in the contemporaneous liquid, the resulting fraction $p_r(f)$ of the residual porosity allotted to feldspar, and the An range. The "*l*" leg of the lever defines the bulk composition of the trapped liquid. The An range defines the total

amount of crystallization until the local system is solidified.

For the LZ example, the An range is 19 mol % An, and the solidification process occupies about 20 % of the normalized temperature range. The latent and sensible heat for this history of solidification is extracted solely through the floor, because the latent heat hump (Morse, 1986) at the floor of the magma chamber is at a thermal maximum and isolates all parts of the cumulate edifice below so that they lie in the sub-floor gradient.

For the UBZ example, the relationships are crowded but essentially the same as for the LZ example. The residual porosity is 36%, the An range 20 %, and the other parameters are as listed. The actual feldspars are projected from Or and consist of oligoclase being resorbed by sanidine in the odd reaction *L* = San - Pl.

The thermal history of the Kiglapait Lower Zone example in Fig. 3 can be quantified with the help of the *T*-*X* plot of Fig. 4, based on the experimental study at 5 kbar by Morse et al. (2004). This figure contains all the available data for plagioclase compositions paired with liquidus temperatures, in which the direct determinations of the plagioclase crystal compositions in glass are shown as black filled circles, and the plagioclase compositions calculated from plagioclase - liquid partitioning data are plotted as grayscale circles. For the sample KI 3660 (13 PCS) in Fig. 3, the An range is 19 mol % An, running from An_{69} to An_{50}, hence occupying all of the territory of Fig. 4, for a thermal path of 60°C.

Fig. 5 shows the relations for smaller values of the An range in the LZ at 10 PCS and the UZ at 93.7 PCS. As the An range decreases to nothing, the residual porosity also goes to zero and the rocks are adcumulates, of which there are many in Fig. 1. The temperature range for the LZ sample at 10 PCS is 16.8°C, as discussed in the caption to Fig. 5.

Skaergaard examples

The data for the An range and residual porosity for the Skaergaard intrusion are shown in Fig. 6, adapted from Fig. 17b of Morse (2012). The individual data points, mainly from Maaløe (1976) and Toplis et al. (2008), are shown as filled circles in black for the An range and gray for the residual porosity. The gray line in the LZ is not a regression on the data shown here, but instead on the residual porosity calculated from the phosphorus data of Tegner et al. (2009) plotted against the *X* axis. It confirms that the calculation of the individual points from the An range is roughly consistent with the input data from Tegner et al. in this stratigraphic region. The

high values of porosity in and above the MZ are from the detailed measurements of the An range by Toplis et al. (2008), and are considered definitive in this region where the criteria of Tegner et al. (2009) are based on elements that are no longer truly excluded.

The solidification calculations for two of the highest values of residual porosity circled in Fig. 6 are shown in Fig. 7. These follow the same protocols as in the previous Kiglapait figures, but the binary loop here is taken from the 1-atm system Di-An-Ab as discussed in Morse (1997), in order to reflect the nominally lower-pressure condition of the Skaergaard crystallization compared to Kiglapait. The relevant data are given in the diagram as before, so the solidification process can be followed by walking through the figure. Diagrams showing cases with lower values of the residual porosity are similar to those shown in Fig. 5 and need not be repeated here for Skaergaard. The temperatures for the synthetic system are higher than for the actual Skaergaard magma, but the temperature differences for the solidification may be approximately correct. They are in the range of ~15-20˚C for these orthocumulates.

DISCUSSION

Failed correlations

The premise of using the An range to calculate residual porosity rests on the observation that the two measures correlate with each other. This correlation is missing in the extreme limits of An content in Table 2 of Humphreys (2009). The five samples concerned are from the Hidden Zone, LZA, and LZb of the Skaergaard intrusion. The data, shown in Fig. 8, are for the An range calculated from the maximum core and minimum rim compositions. When the maximum An range is plotted against the residual porosity calculated from the phosphorus data of Tegner et al. (2009), there is no meaningful correlation (Fig. 8).

Comparison of the compositional data with the An ranges shown in Fig. 7 may be helpful in understanding this result. The maximum values of An% = ~74-64 overlap the LZA range of ~69-55 in Fig. 7, so are apparently about normal for the HZ-LZb range. The minimum values ~54-31 are abnormally low for typical HZ-LZb samples, and barely overlap with the upper values of UZb in Fig. 7. In short, they occupy the middle part of the diagram.

The two lowest values of the An range, 11.7 and 15 mol % An (Fig. 8), give results for the residual porosity of 32 and 41 %, respectively, and these are high but not abnormal for the HZ-LZ range shown in Fig. 7. The three high values of the An range give nominal values of the

residual porosity 90 - 108 %, and are clearly abnormal in their minimum values of extremely evolved rims. Note that rims of such a composition as An_{31} would not be abnormal for a UZb rock (Fig. 7). One may only conclude that these three HZ-LZ rocks are unusual in their extremely evolved rims for that stratigraphic level, and that some explanation other than solidification of a simple, contemporaneous trapped liquid must apply here. Some insight into this problem may emerge from the end of the next section of this paper on melt inclusions.

MELT INCLUSIONS

Introduction

There is a fundamental difference between trapped liquid in a cumulate and a melt inclusion. In a cumulate, the liquid that is trapped is the parent magma that deposited the last of the cumulus plagioclase. If the rock is an orthocumulate, the unmodified parent magma occurs in contact with the interstitial magma and they are both the same. If there has been an interval of adcumulus growth, then there has been a constant exchange reaction in which isothermal crystal growth has occurred, and therefore the contact magma has been continuously exchanged, so the trapped liquid represents closure of the parent magma. That closure process, incidentally, is what permits the estimation of residual porosity by consideration of excluded components, as done by Wager (1963) and many others since (e.g., Morse, 1979; Tegner et al., 2009).

A melt inclusion is a liquid that has been trapped by a single growing crystal, or conceivably in the junction between two growing crystals of the same species, one of which has eventually outgrown the other. Crystal growth occurs by the rejection of solute that is not part of the contemporaneous crystal composition. (It is this solute that is continually exchanged with the parent magma during adcumulus growth.) The growing crystal lies within a sheath or envelope of that solute, which is continuously removed at some distance by diffusion and convection. The typical growth spikes found in experiments (e.g., Morse et al. 2004) at the corners of growing crystals represent, in effect, the attempt by the crystal to reach out past the sheath to find common cause in the unevolved melt. When a crystal then grows so fast that it captures and includes a sample of the adjacent melt, is has by definition sampled the evolved sheath. It is highly probable, therefore, that the melt inclusion will represent the local sheath of evolved melt, not the more distant fresh melt. Solute rejection is discussed in formal treatments of

crystallization, such as Gordon (1968) or Tiller (1991) as in his Fig. 1.7. Trapping of liquid by crystal growth is also discussed by Tiller (e.g., Fig. 4.17 ff) and in the petrologic literature by Walker and Agee (1989).

After trapping by the crystal, the evolved melt undergoes further evolution until it is solidified. The principles of solidification are exactly those of the trapped liquid in a cumulate, with the plausible difference of a starting point that is not in secular equilibrium with the parent magma, but with an evolved product of that magma.

Experimental

Recent experimental results may help to illustrate the effect of the boundary layer in the ultimate composition of a melt inclusion. In a program designed to explore the mantle origin of the Kiglapait magma following the experimental protocols of (Morse et al. 2004 and McIntosh 2009), excess Mg-rich olivine was added to the estimated bulk composition of the intrusion and the finely ground mixtures were melted in graphite at 13 kbar. Experiment No. KI-PM2 was held at 13 kbar pressure and 1375°C for 3.5 h. The experiment began at 1475°C and was lowered at 1.9°C/min to the final temperature. The superheating is assumed to have destroyed all crystal nuclei in the original finely ground crystalline mixture. In two of the bulk compositions studied, rare crystals of olivine occur, and a few of them contain melt inclusions. Data for two of the compositions are given in Table 1with normative plotting conventions as defined in Morse et al. (2004). An image of a euhedral olivine in composition BC35 is shown in Fig. 9. The crystal occurs near the edge of the charge against the graphite container (black in the figure), along with feathery dendrites interpreted as quench crystals of olivine. A shear zone of dislocations running through the image is assumed to have formed during or after the quench.

The data in Table 1 show that the melt inclusion is far from equilibrium with the surrounding olivine, with a K_D of 0.15 compared to the $K_D = 0.39$ for the bulk olivine paired with the surrounding glass. The melt inclusion is strongly enriched in the components of plagioclase, and a ternary plot (Fig. 10) shows that it lies close to the plagioclase - olivine cotectic. It is assumed that the inward growth of the host olivine has helped to increase the evolution of the melt in the inclusion; nevertheless, the two are not in equilibrium. Clearly, the melt inclusion is far from representing the bulk liquid sampled in the hinterland of the crystal, and this is expected to be the general rule for melt inclusions. The host crystal grew at a mean

rate of ~25 cm y^{-1}.

Application to a Skaergaard example

It is pertinent to apply the principle of the An range as a measure of residual porosity to melt inclusions hosted in plagioclase. A test case involving the Skaergaard intrusion can be of value because of the abundant information already at hand in that occurrence as reflected in Fig. 6.

In a treatment by Jakobsen et al. (2011), the authors have discovered abundant melt inclusions in Skaergaard plagioclase, from which they infer the primary coexistence of an emulsion of immiscible evolved and refractory liquids in the parent magma at early stages (LZc) of crystallization.

Among the well-illustrated relationships of inclusions to their plagioclase hosts is at least one example (Fig. 3e in the original) of "optical zoning in plagioclase around a melt inclusion." The variation of plagioclase compositions within melt inclusions is presented in their Table 2, along with the compositions of host crystals away from inclusions. It is not clear that any but a few host crystals show zoning toward the inclusions. Taking the simplest interpretation, it is reasonable to regard the difference between the mean composition of a distant host and the least An content within the nearby inclusion as an An range subject to the Skaergaard equation for the interpretation of the residual porosity.

There are six examples in their Table 2 of hosts away from inclusions paired with melt inclusions, for each of which 3 or 4 measurements are given. The resulting maximum An ranges are, in stratigraphic order within the stratigraphic interval LZc to MZ, 5.4, 2.8, 6.2, 9.1, 12.3, and 17.8 mol % An. Most of these values are similar to what we have already encountered in an examination of Skaergaard residual porosity (Fig. 6). The corresponding conversion to residual porosity for the Skaergaard intrusion (Morse, 2012) results in values ranging from 10 to 48%, and these are plotted as black triangles on the Skaergaard diagram in Fig. 6. The first four points in LZc and MZ faithfully follow the conventional values for residual porosity as interpreted from excluded components and from the calibrated An range. The fifth point is higher, at a value of 34% in porosity, than other MZ values, but not unlike the high UZ values. The sixth point, at a value of 48%, is unusual, possibly signifying capture of an abnormally evolved sheath by the rapidly growing crystal. Also of interest is that the two lowest points shadow the decreasing slope of the phosphorus-based residual porosity of Tegner et al. (2009), while all the succeeding

MZ points fall on a steeply sloped, nearly straight line.

The inference to be drawn from this exercise is that there is little if anything unique about the melt inclusion data that is not also compatible with a straightforward principle of the ordinary solidification of trapped liquid, aided at least in part by the capture of an already evolved melt by the growth of a crystal into its evolved surroundings. The appearance of apatite (the Ap^{+} event) in the Skaergaard stratigraphic column occurs at a plagioclase composition of ~ An_{39} (Mcbirney, 1996); of the inclusions in Table 2, the lowest An contents of the most evolved three are An 39, 37, and 30, so each of these inclusions would be expected to contain apatite, as found among the daughter phases. Two others, at An 42 and 45, might also be within range of apatite saturation if the evolved sheath were by chance more evolved in P than in An content. Indeed, the authors report apatite even in the sample with An 50 from LZc, indicating a composition evolved in P.

In short, there is nothing surprising about the melt inclusions as listed in the cited contribution when they are viewed as products of residual porosity, possibly enhanced by the initial evolved characteristic of the melt at the time of trapping. The case for a resident liquid emulsion cannot rest on the evidence if Table 2 of Jakobsen et al. (2011) is characteristic.

Discussion

The cited authors are well aware of the boundary diffusion layer that surrounds growing crystals but consider (p. 362) that the very slow crystallization rates of plutonic plagioclase would render that effect insignificant. The nominal mean growth rate at the Skaergaard intrusion is estimated to be < 2 cm y^{-1}. However, because of the exponential nature of heat loss to the surroundings, the actual accumulation rate in the very early history of a layered intrusion might reach values as high as 20 cm y^{-1} in the first few hundred years or after a local marginal slump. Moreover, it is not always certain that crystal growth is a steady-state rate rather than a fluctuating rate between spurts of rapid nucleation followed by slower growth.

For example, crystal growth in general must slow down during the periodic maximal release of latent heat (Morse, 2011), and speed up as that maximal release diminishes. The crystal growth rate should become greatest at the least release of latent heat, just before the arrival of a new cumulus phase. Although the peaks and valleys in the release of fractional latent heat are

indigenous to the entire magma body in the cited study, they also pertain in principle to local events associated with rhythmic layering. In particular, every mafic layer represents an overload of mafic crystals continuing to grow in the mush, releasing a local maximum of latent heat, thereby damping any tendency to nucleation of crystals in the surroundings or in the source plume from the roof. At the end of this process of solidification, rapid nucleation and growth of the pent-up plagioclase component in the overlying liquid may occur, leading to an increased likelihood of trapping melt rapidly.

According to this hypothesis, it would be interesting to learn whether melt inclusions in Skaergaard plagioclase may more often occur immediately above mafic layers.

Source of the failed correlation

As to the problem of the extremely evolved rims discussed in connection with Fig. 8, it appears plausible that these, too, may represent jumps into an evolved sheath, a process in which the cumulate mimics the effect of crystal growth. This might happen, for example, if the crystallization rate at the floor was suddenly increased. Such a condition might occur when a protective, latent-heat producing layer was suddenly stripped away by gravitational collapse, a process most likely to occur early in the history of the intrusion, and near the walls (Humphreys and Holness, 2010).

THE LOST RESIDUE

The Kiglapait intrusion bulk composition has K_2O = 0.22 wt % (Morse, 1981) and ends up at the ternary feldspar minimum with sanidine growing at the expense of oligoclase (Morse, 1969 Fig. 3 Plate 49). The Skaergaard intrusion bulk composition has K_2O = 0.40 wt % (Nielsen, 2004) and ends up in the oligoclase composition range without any K-feldspar. Why this difference? Our present investigation can shed light on this nagging perennial question.

The rising end-stage residual porosity in both intrusions is evident from the An range in plagioclase (Morse, 2012) and Fig. 6 here. The presence of plagioclase - chain networks at late stages was suggested (Morse, 2012) to have played a role in sequestering liquid that in effect ended in equilibrium crystallization. If we take the An range for the entire intrusion as a basis for understanding the process of solidification, then the end stage represents, in effect, the case of trapped liquid. Thus we have, at Skaergaard, a cessation of feldspar evolution at a local bulk

459 composition constituting the upper parts of UZb, and at Kiglapait, an incongruent reaction near
460 the ternary minimum in which sanidine crystallizes from liquid at the expense of oligoclase.
461 These diverse end points can be attributed entirely to the total history of trapped liquid in the
462 two intrusions. In the Kiglapait intrusion, the residual porosity started low and remained on a
463 decreasing trend until 99 PCS. This trend means that the efficiency of fractionation was high,
464 nearly optimum, because trapped liquid has a partition coefficient of 1.0 for all components. By
465 the same token, the residual porosity at Skaergaard was initially very high and, although it
466 decreased to low values, the minimum residual porosity occurred at ~60-70 PCS (Fig. 6), after
467 which it varied from low to high, becoming high after 80-90 PCS. In effect, the trapped liquid
468 continually sequestered the K-rich feldspar component (and its associated Ba and Sr), leaving
469 nothing much at the end. The final stages of Skaergaard crystallization were similar to
470 equilibrium crystallization, but more accurately were simply the effect of the total solid
471 composition becoming equal to the bulk composition at oligoclase. By contrast, the Kiglapait
472 late feldspars became exceedingly rich in Sr (670 ppm; Morse, 1982) and Ba (1.42 %; Morse, in
473 preparation).
474 The moral for the health of layered intrusions: Too much trapped liquid is bad for your
475 residue.
476
477 **CONCLUSIONS**
478
479 The solidification of trapped liquid in an igneous cumulate is a function of its volume (the
480 residual porosity) and time and temperature. The range of plagioclase composition displayed in
481 the cumulate provides a quantitative measure of that history by use of the lever rule in binary
482 solutions. Such a range is best determined by use of grain mounts separated from large volumes
483 (> 10 cm^3) of sample. The trapping of melt by crystal growth is a different process in that it most
484 likely captures the evolved sheath of rejected solute and therefore begins life already evolved.
485 When that principle is applied to melt inclusions in Skaergaard plagioclase, it appears likely that
486 the evolved crystallized melt inclusions result from the relative speed of capture and need not
487 represent a pervasive emulsion of immiscible liquid. Aberrantly evolved rims in three
488 Skaergaard cumulates may also have resulted from rapid capture consequent upon the sudden
489 removal of a thermal blanket. The differing end-stage histories of fractionation in the two
490 intrusions can be attributed entirely to their differing histories of residual porosity, in which the

low-melting components of feldspar were sequestered in the Skaergaard trapped liquid instead of being enriched to the end of crystallization, as at Kiglapait.

ACKNOWLEDGMENTS

I am grateful to the interested reader who triggered this analysis. A preview by Brian O'Driscoll was most helpful in the improvement of the manuscript. External reviews resulted in a significant re-organization of the presentation.

This article is based on research supported by NSF under Award No. EAR 0948095.

REFERENCES CITED

Humphreys, M. C. S. (2009) Chemical evolution of intercumulus liquid, as recorded in plagioclase overgrowth rims from the Skaergaard intrusion. Journal of Petrology, 50, 127-145.

Humphreys, M. C. S. and Holness, M. B. (2010) Melt-rich segregations in the Skaergaard Marginal Border Series: Tearing of a vertical silicate mush. Lithos, 119, 181-192.

Gordon, Paul (1968) Principles of phase diagrams in materials systems. New York: McGraw Hill.

Grove, T. L., Baker, M. B., Kinzler, R. J. (1984) Coupled CaAl-NaSi diffusion in plagioclase feldspar: Experiments and applications to cooling rate speedometry. Geochimica et Cosmochimica Acta, 48, 2113-2121.

Jakobsen, J. K., Veksler, I. V., Tegner, C., Brooks, C. K. (2011) Crystallization of the Skaergaard Intrusion from an emulsion of immiscible iron- and silica-rich liquids: Evidence from melt inclusions in plagioclase. Journal of Petrology, 52, 345-373.

Maaløe, Sven, (1976) The zoned plagioclase of the Skaergaard Intrusion, East Greenland. Journal of Petrology, 17, 398-419.

McBirney, A. R. (1996) The Skaergaard Intrusion. In: Cawthorn, R. G. (ed.) Layered Intrusions. Amsterdam: Elsevier, pp. 147-180.

McIntosh, D. C. B. (2009) An experimental study exploring the magmatic source region of the Kiglapait layered intrusion, Labrador, Canada. MS thesis, University of Massachusetts, 93 pp.

M^{c}Kenzie, D. (2012). Compaction and crystallization in magma chambers: Towards a model of the Skaergaard intrusion. Journal of Petrology, 53, 905-930.

Morse, S. A. (1969) The Kiglapait Layered Intrusion, Labrador. Geological Society of America Memoir 112, 204 pp.

Morse, S. A. (1979) Kiglapait geochemistry II: Petrography. Journal of Petrology, 20, 591-624.

Morse, S. A. (1981) Kiglapait geochemistry IV: The major elements. Geochimica et Cosmochimica Acta, 45, 461- 479.

Morse, S. A. (1984) Cation diffusion in plagioclase feldspar. Science, 225, 504- 505.

Morse, S. A. (1986) Convection in aid of adcumulus growth. Journal of Petrology, 27**,** 1183-1215.

Morse, S. A. (1997) Binary solutions and the lever rule revisited. Journal of Geology, 105, 471-482.

Morse, S. A. (2000) Linear partitioning in binary solutions. Geochimica et Cosmochimica Acta, 64, 2309-2319.

Morse, S. A. (2011) The fractional latent heat of crystallizing magmas. American Mineralogist, 96, 682-689.

Morse, S. A. (2012) Plagioclase An range and residual porosity in igneous cumulates of the Kiglapait Intrusion. Journal of Petrology, 53, 891-918.

Morse, S. A., Nolan, K. M. (1984). Origin of strongly reversed rims on plagioclase in cumulates. Earth and Planetary Science Letters, 68, 485-498.

Morse, S. A., Brady, J. B. and Sporleder, B. A. (2004) Experimental petrology of the Kiglapait intrusion: Cotectic trace for the Lower Zone at 5kb in graphite. Journal of Petrology, 45, 2225-2259.

Nielsen, T. F. D. (2004). The shape and volume of the Skaergaard intrusion: implications for mass balances and bulk composition. Journal of Petrology, 45, 507-530.

Tegner, C., Thy, P., Holness, M. B., Jakobsen, J. K., and Lesher, C. E. (2009) Differentiation and compaction in the Skaergaard Intrusion. Journal of Petrology, 50, 813-840.

Tiller, W. A. (1991) The science of crystallization: microscopic interfacial phenomena. Cambridge University Press, 391 pp.

Toplis, M. J., Brown, W. L., and Pupier, Elsa (2008) Plagioclase in the Skaergaard intrusion: Part 1: Core and rim compositions in the Layered Series. Contributions to Mineralogy and Petrology, 155, 329-340.

Wager, L. R. (1963) The mechanism of adcumulus growth in the Layered Series of the Skaergaard intrusion. Mineralogical Society of America Special Paper, 1, 1-9.

Walker, D. and Agee, C. (1989) Partitioning “equilibrium”, temperature gradients, and constraints on Earth differentiation. Earth and Planetary Science Letters 96, 49-60.

Wyllie, P.J. (1963) Effects of the changes in slope occurring on liquidus and solidus paths in the system diopside-anorthite-albite. Mineralogical Society of America Special Paper, 1, 204-212.

Figure Captions 15 December 2012

FIGURE 1. Residual porosity of single samples in the Kiglapait intrusion, based on Fig. 11 of Morse (2012). The *X* axis is volume percent solidified (PCS) recalculated as the negative log of the fraction of liquid remaining. The dotted lines simply call attention to the upper limits of the data points. The heavy continuous curve is the intrusion model. The horizontal dashed line calls attention to the ~15 samples with very low porosity; values lower than zero arise from pre-cumulus zoning. The data points and model are calculated from the An range as shown in the equation.

FIGURE 2. Distorted binary plagioclase loop (K_D = 0.2; Morse, 2000) showing the principle of the relationship between residual porosity and the An range. For an An range of 21 mol %, the instantaneous solid composition (ISC) follows the solidus curve as shown by the heavy line labeled "xl zoning." In company, attached to the horizontal tie lines, the trapped liquid follows the heavy line on the liquidus. The bulk composition BC is found from an arbitrary equation for a fictitious residual porosity, $Y = 2.2\ X - 21$ where X = the An range. The result expressed as a fraction defines the length of the *l* leg of the lever *s* + *l*, where the letters stand for solid and liquid, respectively. The total solid composition (TSC) runs from the initial solidus composition to a point on the bulk composition at the last temperature defined by the limit of the An range, at which point the liquid is all consumed. This demonstration ignores the role of the mafic component, which is elaborated in the text and subsequent diagrams.

FIGURE 3. Solidification of trapped liquids from two samples with high porosities in the Kiglapait intrusion. The loop shown is a generic binary loop with linear partitioning K_D = 0.416 (Morse, 2000) appropriate to a mean pressure of 3 kbar. For each sample the sample numbers, PCS values, residual porosities, feldspar fractions, reduced residual porosity p_r(f) due to feldspar alone, and An range are given. The An range defines the interval of composition and temperature over which the trapped liquid solidifies. It is assumed that all mafic phases re-equilibrate by reactive equilibrium crystallization, whereas the plagioclase solidifies only by zoning. The feldspar fraction of the residual porosity defines the liquid leg *l* of the lever *(s+l)* and thereby also defines the bulk composition BC of the residual liquid in terms of the feldspar component. The trapped liquid follows the bold path on the liquidus and the instantaneous solid composition

(ISC; "xl zoning") follows the bold path on the solidus. The total solid composition TSC follows the dotted path from the initial solidus composition to a point on the bulk composition line that is defined by an extended lever from the final liquid composition. Labels: BC, bulk composition; TSC, total solid composition; s and l, solid and liquid legs of the lever. The An range is shown by the labels between vertical lines. The *Y* axis of the figure is normalized temperature and not useful in practice, but the experimental range for the sample at 13 PCS is 60°C from Fig. 4.

FIGURE 4. Experimental liquidus temperatures at 5 kbar for the Kiglapait Lower Zone based on the experimental data of Morse et al. (2004), with crystal compositions measured (black filled circles) and calculated (gray circles) from the liquid compositions contained in that paper. The calculations were made from the equation $D(X\text{Ab}) = K_D\,(X\text{An}^S) + X\text{Ab}^S$ where $D = X_{Ab}(\text{Plag})/X_{Ab}(\text{Liq})$ and $K_D = 0.524$. The concave-up nature of the curve is consistent with the Wyllie (1963) principle of shelves having lower slope in *T*-*X* space when a new phase (here augite) is added to the crystalline mixture; see Morse (2011). This diagram is valid only for troctolitic liquids in the range of plagioclase composition shown. For the case of Fig. 3, the entire range from An_{69} to An_{50} is encountered, giving a range of 60°C.

FIGURE 5. Solidification of trapped liquids from two Kiglapait samples with small residual porosity. Labels as in Fig. 3. The experimental range from $An_{61.5}$ to An_{51} (as in sample KI 3661) occurs over a range of 16.8°C. Note that sample KI 3661 in this figure is stratigraphically below (10 PCS) that of the sample KI 3660 (13 PCS) with a large temperature range in Fig. 3. This difference reflects the differences in amounts of trapped liquid but also in maximum An content, with the result that the lower sample will have solidified earlier than the overlying sample, but at the same temperature while cooled through the floor.

FIGURE 6. An range (solid symbols) and residual porosity (grayscale symbols and lines) in the Skaergaard intrusion, adapted from Fig. 17b of Morse (2012). Labels: (LZ), Lower Zone; MZ, Middle Zone; UZa, Upper Zone a; Ap+ appearance of apatite. The analysis of solidification to be discussed is related to two samples (circled) with high values of the An range in the LZ and upper UZ. The black triangles ascribed to Jakobsen et al. are described in a separate section on melt inclusions.

655 **FIGURE 7**. Solidification of trapped liquid in two samples of the Skaergaard intrusion. Labels
656 and principles as in the Kiglapait figures (3 and 5). The loop is that of the plagioclase - diopside
657 cotectic in the 1-atm phase diagram of the system Di-An-Ab as analyzed by Morse (1997).
658 Although the temperatures shown are too high for the natural rocks, the temperature differences
659 near 20°C are probably realistic.
660
661 **FIGURE 8**. Example of failed correlation in five Skaergaard rocks with local, highly evolved
662 plagioclase rims as reported by Humphreys (2009). The correlation with residual porosity is
663 deemed not significant, for reasons discussed in the text.
664
665 **FIGURE 9**. Back-scattered electron image of an olivine crystal surrounded by glass in an
666 experiment No. KI-PM2, BC-35 held in graphite at 13 kbar pressure and 1375°C for 3.5 h in the
667 Five College Experimental Petrology Laboratory at Smith College, 28 April 2012. The
668 experiment began at 1475°C and was lowered at 1.9°C/min to the final temperature. The
669 superheating is assumed to have destroyed all crystal nuclei in the original finely ground
670 crystalline mixture.
671
672 **FIGURE 10**. Compositions of experimental glass, olivine, and melt inclusion in the experiment
673 illustrated in Fig. 9; electron probe analyses by Prof. M. J. Jercinovic. The figure is a ternary plot
674 of the oxygen-normative components feldspar (FSP) augite (AUG) and olivine + hypersthene
675 (OLHY) showing the evolved nature of the melt inclusion compared to the parent liquid
676 represented by the glass. The field boundaries are approximate but based on the LZ results of
677 Morse et al. (2004).

This is a preprint, the final version is subject to change, of the American Mineralogist (MSA)
Cite as Authors (Year) Title. American Mineralogist, in press.
(DOI will not work until issue is live.) DOI: http://dx.doi.org/10.2138/am.2013.4327

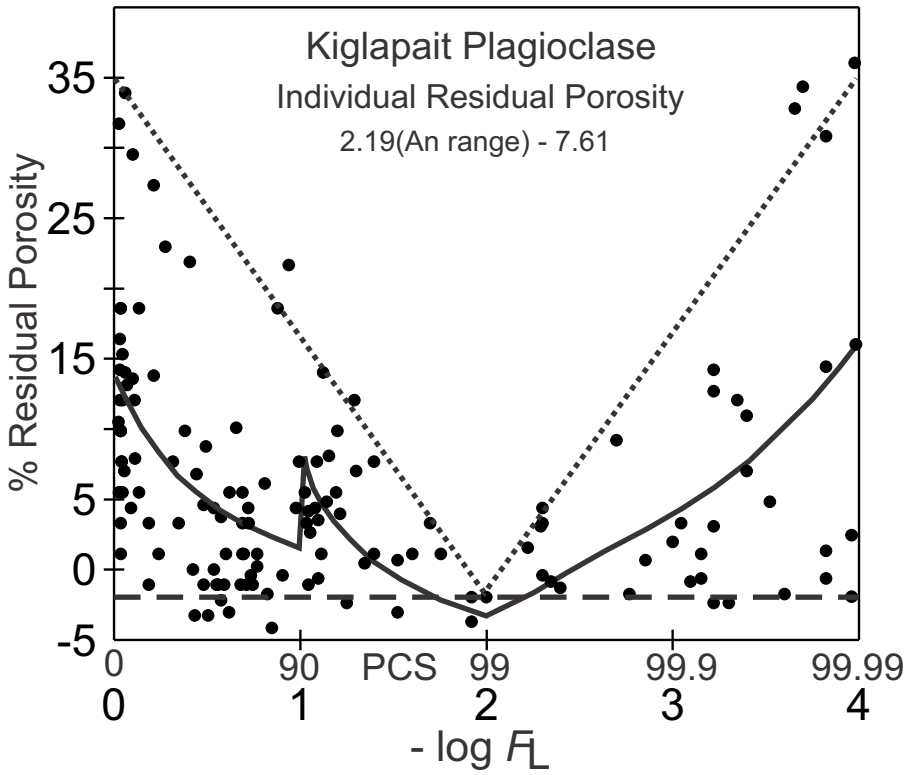

Kipr Calc Modl 09

Morse STL Fig 1

This is a preprint, the final version is subject to change, of the American Mineralogist (MSA)
Cite as Authors (Year) Title. American Mineralogist, in press.
(DOI will not work until issue is live.) DOI: http://dx.doi.org/10.2138/am.2013.4327

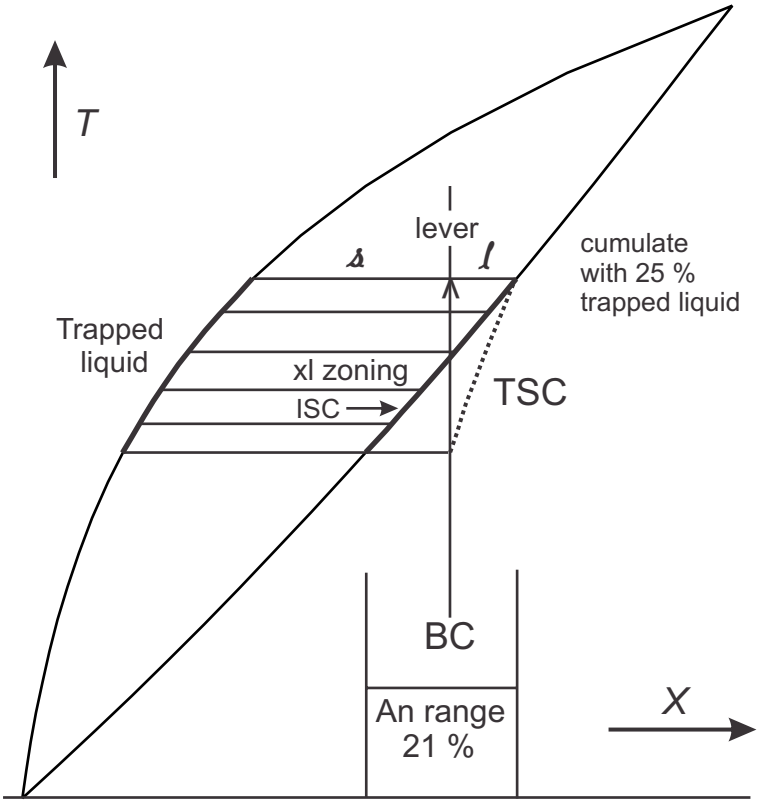

Morse STL Fig. 2

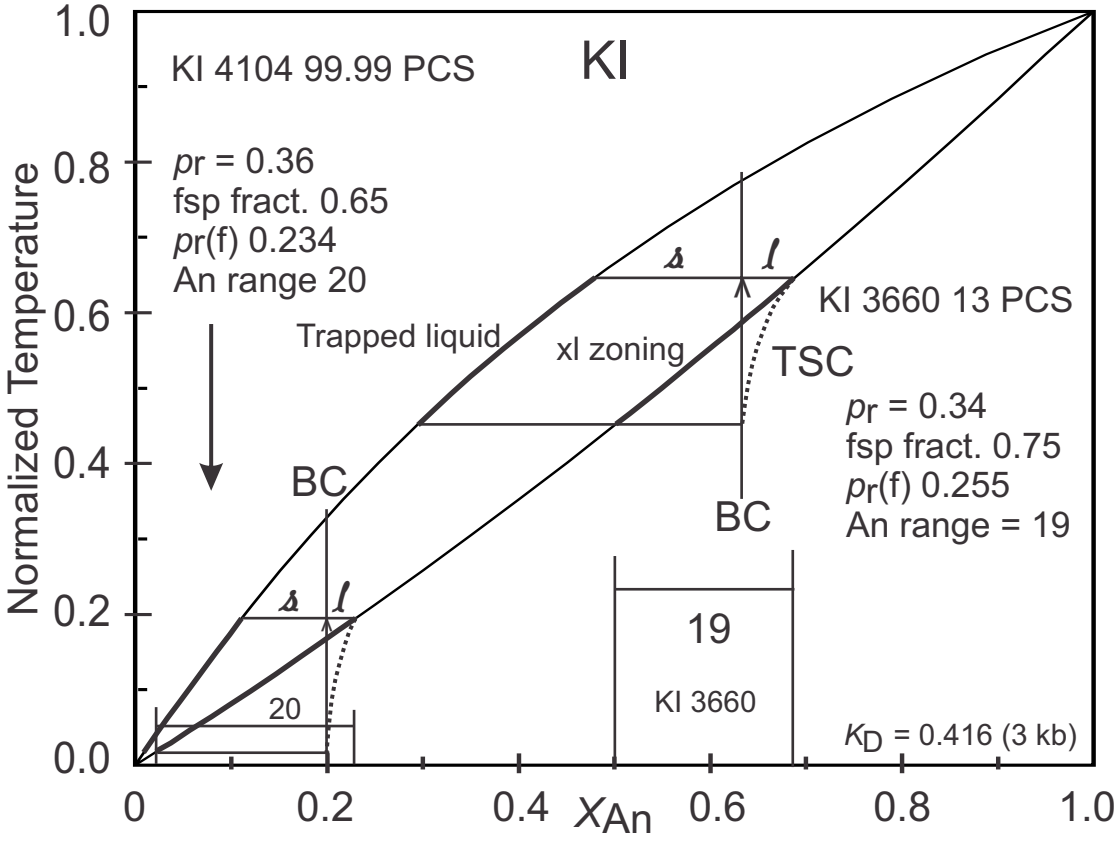

Morse STL Fig 3

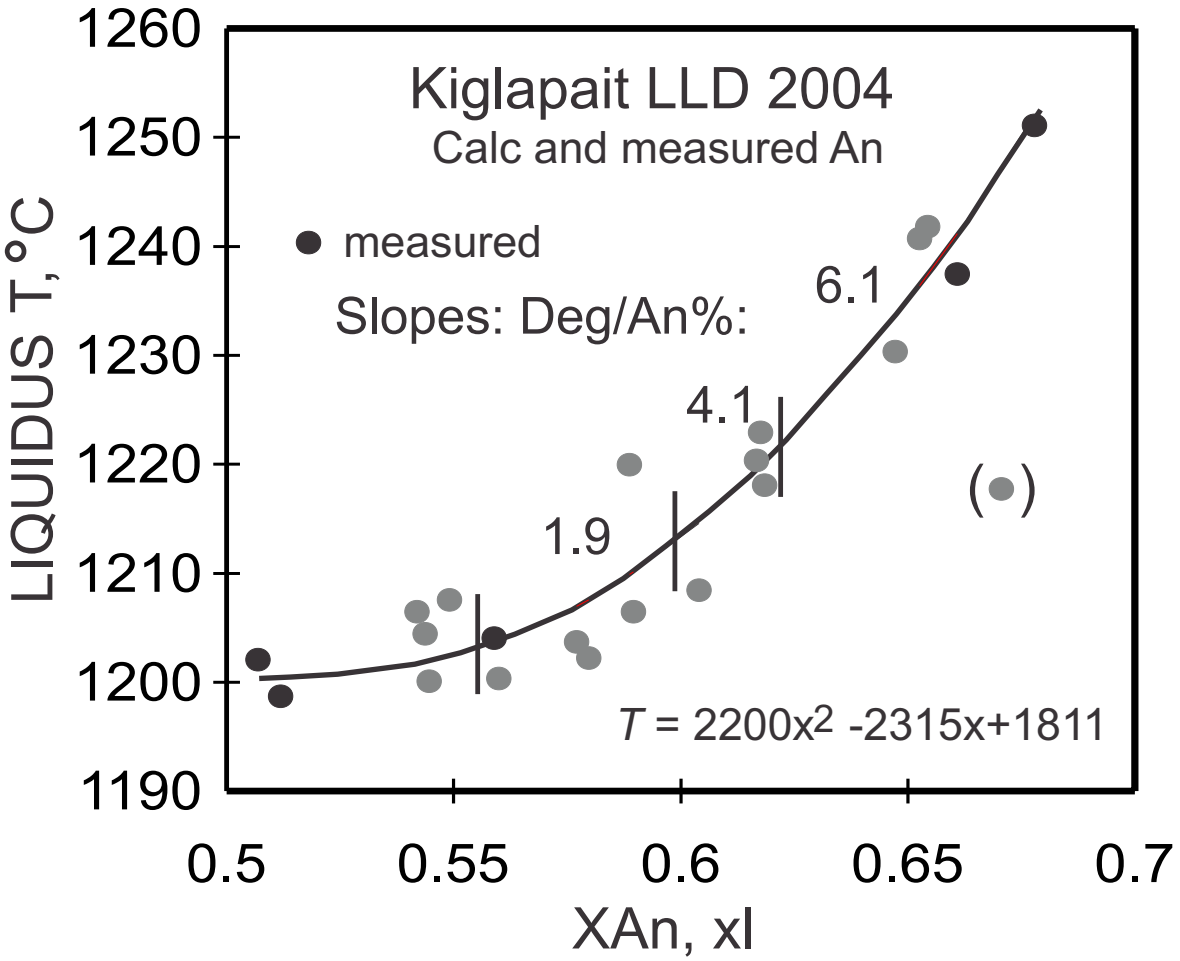

T on XAn 2010a in KI T 3-5

Morse STL Fig. 4

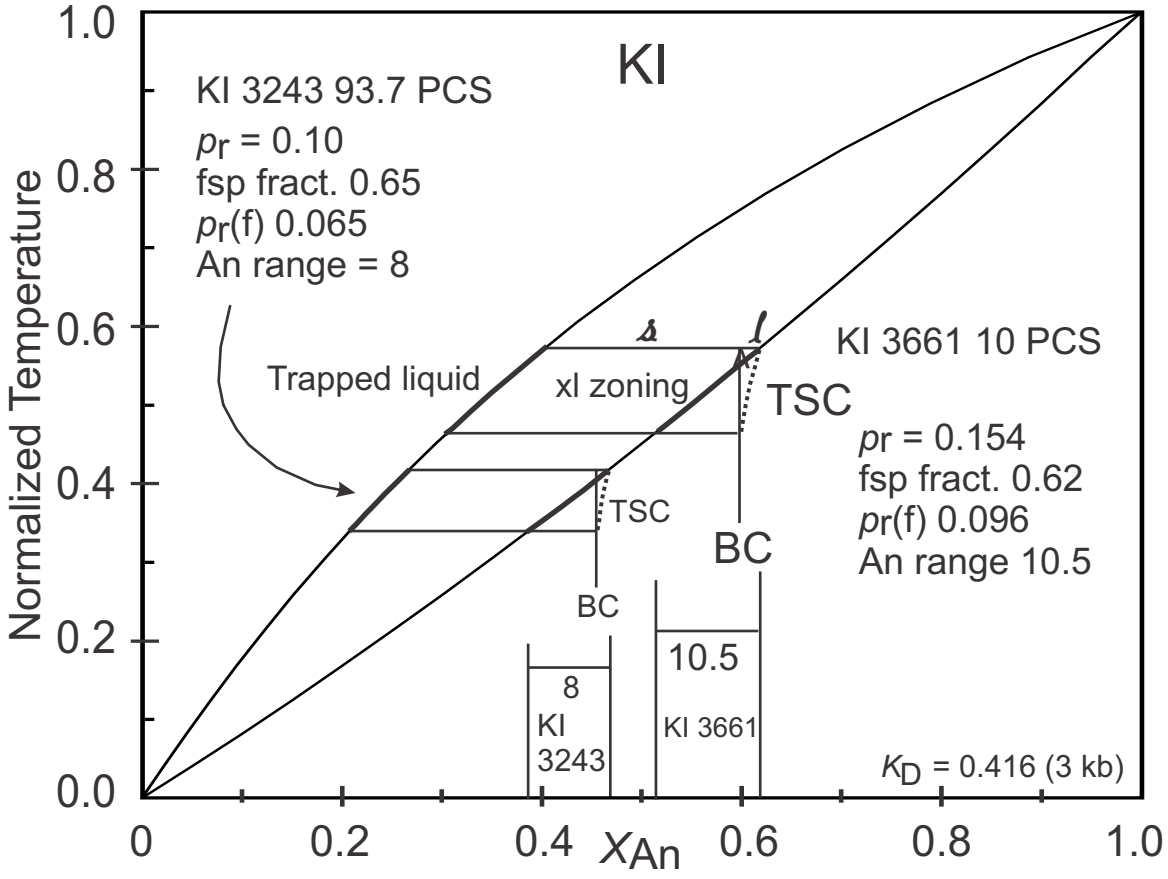

Morse STL Fig. 5

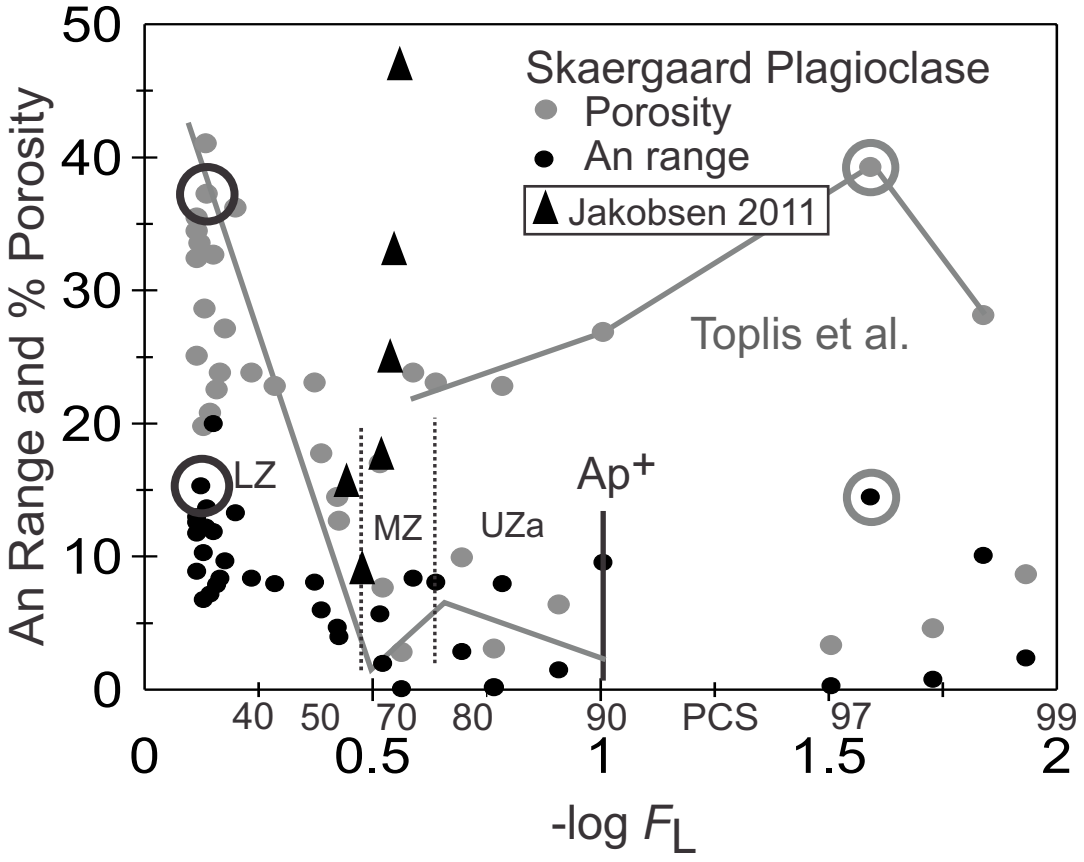

Morse STL Fig 6

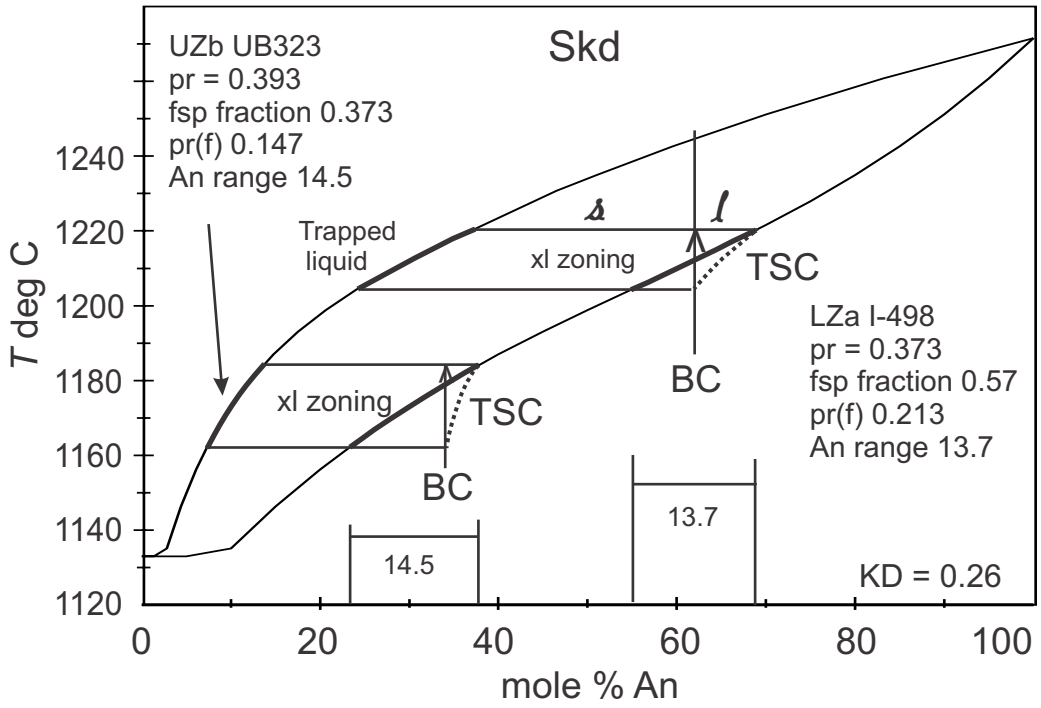

Morse STL Fig 7

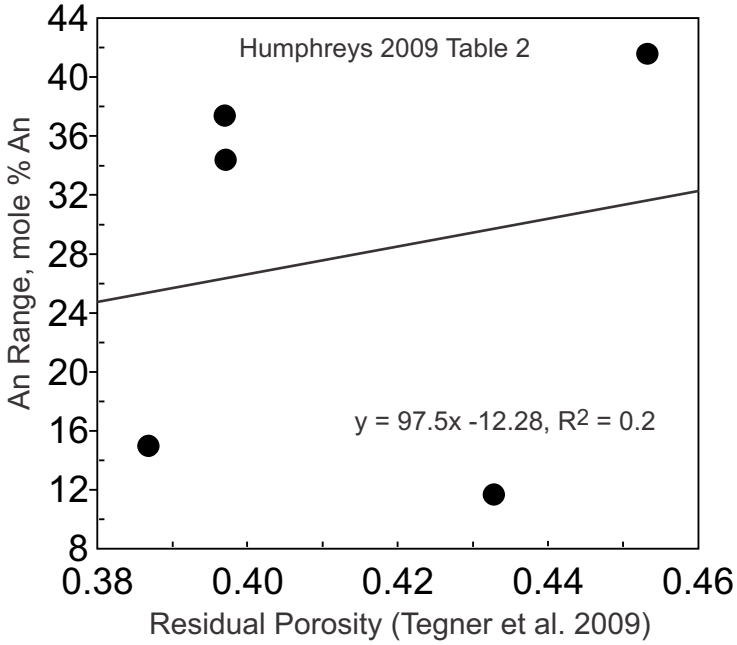

Morse STL Fig 8

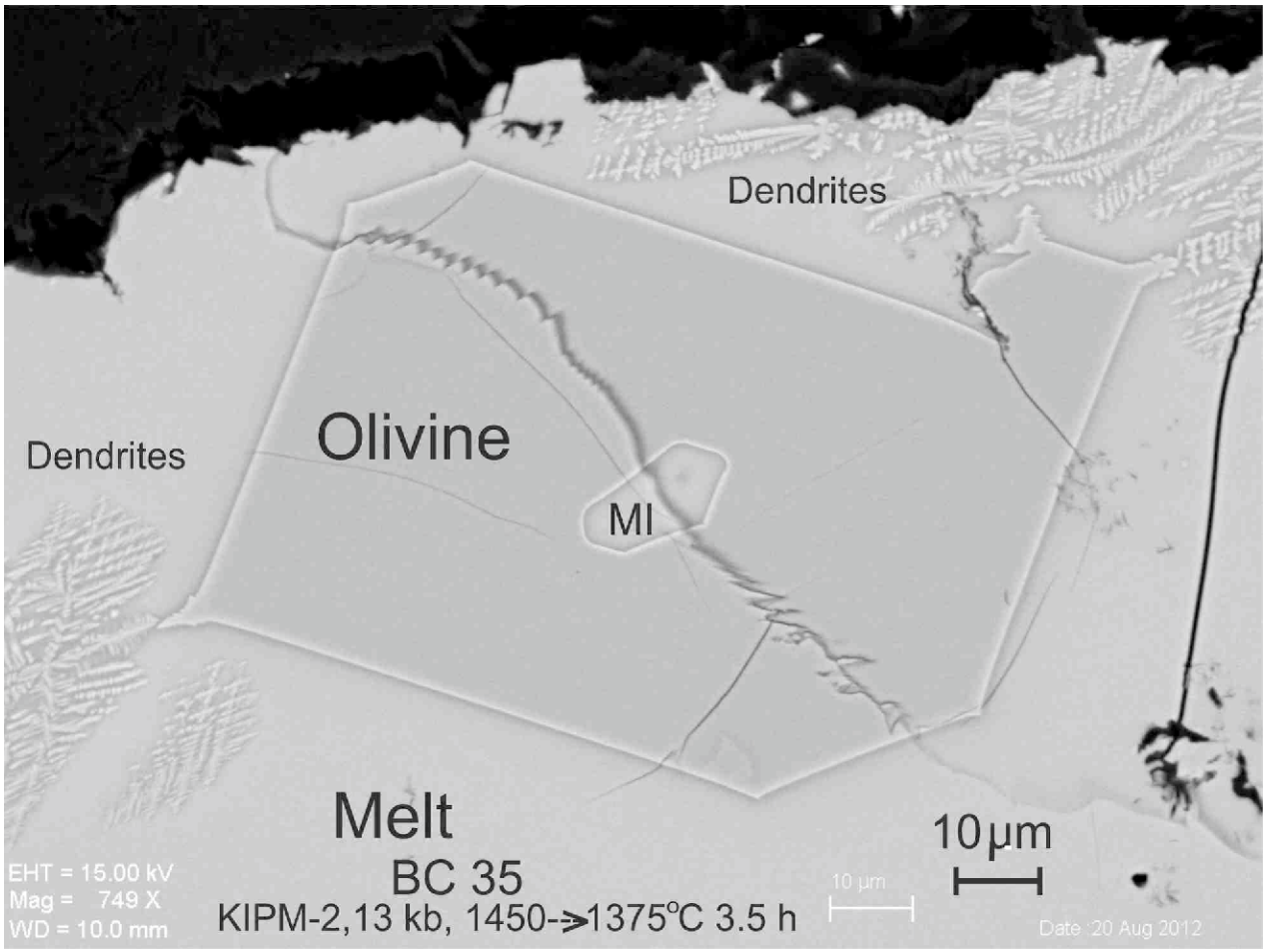

Morse STL Fig. 9

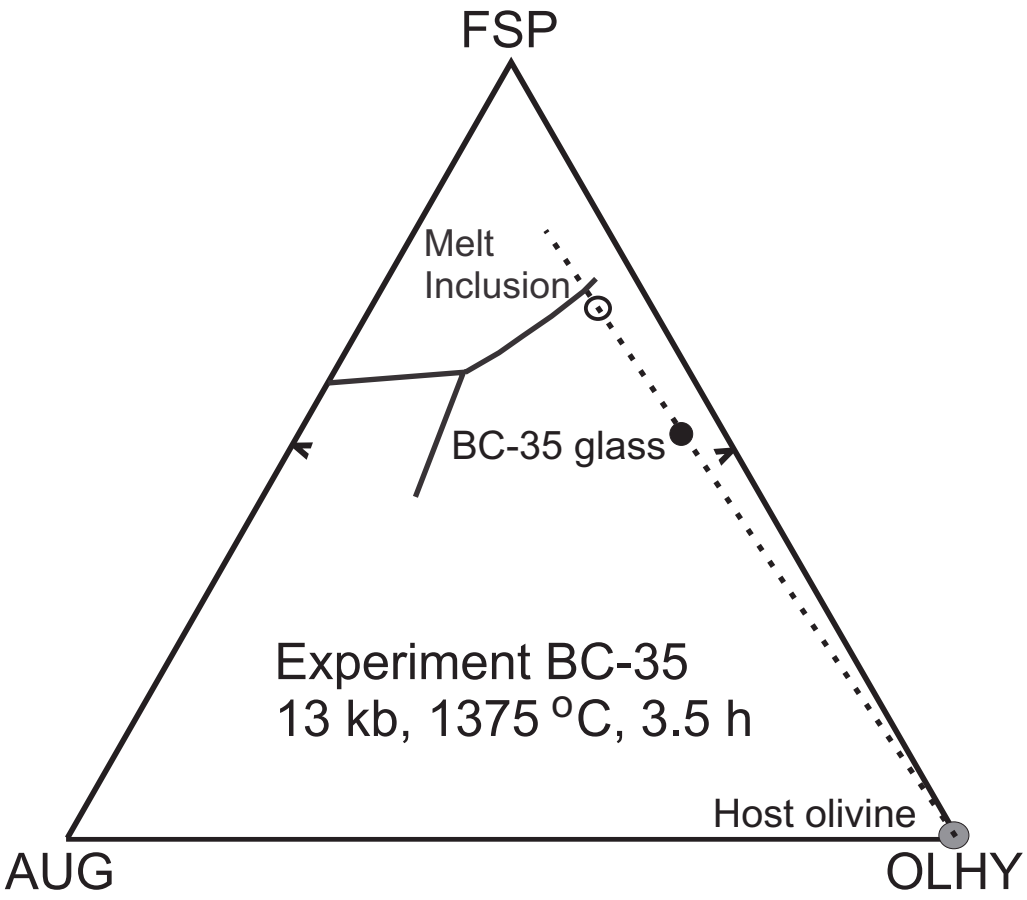

Morse STL Fig. 10

Table 1. Compositions of experimental glass, olivine, and melt inclusions

	Experiment KI PM-2 BC35						Experiment KI PM-2 BC42					
	GLASS		OLIVINE		MELT INCL		GLASS		OLIVINE		MELT INCL	
N = # pts	20		12		5		20		10		10	
	Wt. %	SD	Wt. %	SD	Wt. %	SD	Wt. %	SD	Wt. %	SD	Wt. %	SD
SiO2	48.87	39	40.24	58	50.55	104	49.11	31	40.83	53	51.39	95
TiO2	0.56	5	0.02	2	0.78	6	0.60	4	0.02	1	0.68	4
Al2O3	13.61	16	0.39**	62	17.97	62	13.97	16	0.13**	2	17.75	135
Fe2O3*	1.63	3	0	0	1.42	2	0.01	2	0	0	0.00	0
FeO	13.17	26	17.23	114	11.52	50	13.06	27	14.42	44	11.65	124
MnO	0.18	3	0.15	2	0.22	3	0.15	3	0.13	2	0.16	3
MgO	13.96	23	41.21	192	4.65	38	14.01	27	44.06	43	6.60	153
CaO	6.13	7	0.24	15	8.35	15	6.19	7	0.17	2	7.76	24
Na2O	2.48	2	0	0	3.01	25	2.54	3	0		3.39	48
K2O	0.18	1	0	0	0.22	2	0.19	1	0		0.20	4
P2O5	0.09	4	0	0	0.12	2	0.09	3	0		0.08	3
SUM	100.86	58	99.48	83	98.81	197	99.93	60	99.77	67	99.66	69
	Oxygen Norm						Oxygen Norm					
Mg#	0.65		0.81		0.42		0.68		0.85		0.53	
FSP	52.0		1.1		68.3		53.4		0.4		67.9	
OLHY	43.7		98.9		26.2		42.6		99		26.8	
HY	21.0		--		26.2		22.2		--		22.3	
OL	22.4		98.9		0		20.1		99		4.8	
KD	--		0.39		0.15		--		0.35		0.19	

Note: SD is standard deviation of the last two significant figures.

* Ferrous fraction taken as 0.9 molar for glass and melt inclusions except in calculating KD

** melt overlap